GCAGS JOURNAL
A Publication of the Gulf Coast Association of Geological Societies
www.gcags.org

Volcanic Origin and Significance of Glauconite Grains in the Upper Cretaceous Austin Chalk Formation in the Balcones Igneous Province, South and Central Texas

Robert G. Loucks and Robert M. Reed

Bureau of Economic Geology, Jackson School of Geosciences, The University of Texas at Austin, P.O. Box X, Austin, Texas 78713–8924, U.S.A.

ABSTRACT

Abundant glauconite grains occur in the upper Austin Chalk A and B1 units within the confines of the Balcones Igneous Province (BIP) in the area of the Maverick Basin and San Marcos Arch in Central to South Texas. Controversy exists as to whether the origin of the grains is related to sedimentary hardgrounds or to alteration of volcanic ash and lapilli. The Austin Chalk A and B1 units were deposited contemporaneously with active volcanism (i.e., BIP), and glauconite grains are closely associated with and limited to the area of the BIP. Abundant ash and lapilli are noted near volcanic mounds, where many of these grains are converted to vermiculite and glauconite. It is well established that the BIP pyroclastics underwent alteration in seawater soon after deposition. An unambiguous transition from vermiculite and glauconite-altered volcanic fragments to sand-size glauconite is clearly demonstrated by thin-section and scanning electron microscopy analysis. Grains of glauconite (highly altered ash) deposited away from volcanic mounds have the same origin as those near the mounds. The sand-size glauconite grains can retain internal outlines of gas vesicles and other volcanic microstructures. The misidentification of these volcanic grains as sedimentary-formed glauconite, and not as altered volcanic ash, can lead to misinterpretation of the geologic history and sequence stratigraphy of the upper Austin Chalk section.

INTRODUCTION

Volcanism of the Balcones Igneous Province (BIP) is well documented in the upper Austin Chalk section (B1 unit of Ewing [2013], Loucks et al. [2020], and Loucks and Reed [2022]) in the area of the Maverick Basin and San Marcos Arch in Central to South Texas (Figs. 1 and 2) (e.g., Ewing and Caran, 1982; Ewing, 1986, 2004; Barker et al., 1987; Griffin et al., 2010; Thompson, 2019; Thompson, 2023; Loucks and Reed, 2022). Many volcanic mounds in the Upper Cretaceous Austin Chalk and Taylor formations have been documented by drilling, seismic, and magnetic data, and by outcrop investigations (e.g., Lonsdale, 1927; Luttrell, 1977; Young et al., 1981; Thompson, 1986, 2019; Barker et al., 1987; Mitchell-Tapping, 1988; Ewing, 2004; Saribudak, 2016). In the volcanic detritus associated with and immediately adjacent to the volcanos are ash and lapilli that are altered to vermiculite, glauconite, and lesser phosphate. Distal from the volcanos are silt- and sand-size glauconite grains of similar origin. This distally deposited glauconite is altered volcanic ash, as demonstrated by White (1960), Young et al. (1981), Loucks and Reed (2022), and in more detail in this investigation. Others have interpreted the glauconite grains as sedimentary in origin (e.g., Griffith et al., 2022, 2023). Misidentification of these grains as sedimentary-formed glauconite, and not as altered volcanic ash, can lead to misinterpretation of the geologic history and sequence stratigraphy of the upper Austin Chalk section.

The major goal of this research effort is to document the origin of glauconite grains in the AC–A and –B1 units. Specific objectives are to: (1) review the depositional setting of the BIP in the Maverick Basin and San Marcos Arch, (2) describe the glauconite grains associated with the volcanoes proper and in the distally deposited sediments, (3) verify the transformation of well-preserved vermiculite/glauconite-altered ash and lapilli to smaller silt- and sand-size glauconite grains, and (4) emphasize the importance of a volcanic origin to understanding the geology and regional stratigraphy of the AC–A and –B1 units.

DATA AND METHODS

Basic data for this investigation consist of 12 cores (Table 1) in the AC–A and –B1 units and associated wireline logs from the Maverick Basin to the east side of the San Marcos Arch (Fig. 1). Descriptions of the cores are presented in Loucks and Reed (2022). Thin sections were prepared from the cores to aid in the

Manuscript received May 8, 2023; revised manuscript received July 18, 2023; manuscript accepted July 18, 2023.

GCAGS Journal, v. 12 (2023), p. 1–16.
https://doi.org/10.62371/IIWU2066

Table 1. List of wells with core in the AC–A and –B1 units.

Map #	Well	API#	County
1	Champlin Petroleum Co. No. 1041 H. L. Rogers	42127311640000	Dimmit
2	Proco No. 1 Gise Lawrence	42127328780000	Dimmit
3	Getty No. 1 Lloyd Hurt	42283303050000	Lasalle
4	Tesoro Petroleum Corp. No. 1 J. H. Calvert	42163307280000	Frio
5	Tesoro Petroleum Corp. No. 1 Bryan	42493301770000	Wilson
6	Tesoro Petroleum Corp. No. 1 Valcher	42493302300000	Wilson
7	Prairie Producing No. 1 Wayne Brechtel	42493302080000	Wilson
8	Prairie No. 1 Weinert	4249300000000	Wilson
9	Evergreen Oil Corp. No. 1 Vicker Olyn P.	42177308050000	Gonzales
10	Trans Ocean Oil Inc. No. 2 H. P. Orts	42177302030000	Gonzales
11	Tesoro Petroleum Corp. No. 1 Clare Hendershot	42177302180000	Gonzales
12	Eagle Ford Oil Company No. 1 Clark Sallie	42055018520000	Caldwell

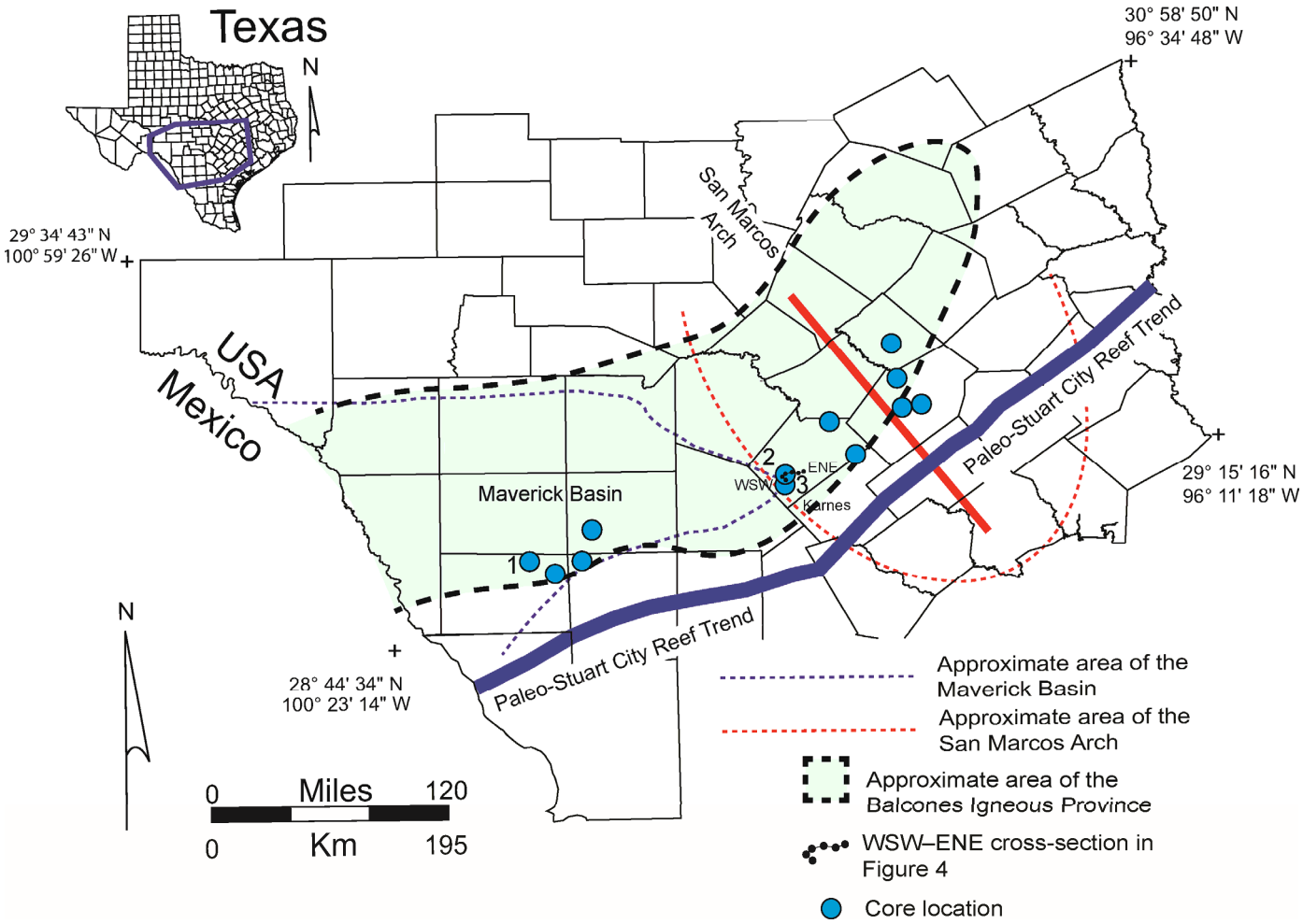

Figure 1. Location map showing outline of the Balcones Igneous Province, Maverick Basin, San Marcos Arch, and the paleo–Stuart City Reef trend. Blue dots are wells with cores in the AC–A and –B1 units discussed in Loucks and Reed (2022). Well 1 is the Getty No. 1 Lloyd Hurt, referred to in Figure 2 and where the wireline log of this well is shown. Wells 2 and 3 are the Tesoro No. 1 Bryan and Tesoro No. 1 Valcher, respectively, which contain cores discussed in this investigation. Location of WSW–ENEcross-section presented in Figure 4 is also shown.

analysis of texture, fabric, mineralogy, and biota. Scanning electron microscopy (SEM) was conducted on selected polished thin sections and Ar–ion-milled samples to define the coccolith-hash matrix and to characterize volcanic material and associated alteration products. An FEI Nova NanoSEM 430 system was used in this investigation. Standard procedures used were an accelerating voltage of 10 to 15 kV with a working distance of 3 to 10 mm. Energy dispersive spectroscopy (EDS) analysis was conducted on selected samples to identify mineralogy at the micrometer scale. Numerous backscattered electron, secondary electron, and EDS images were collected and analyzed.

REGIONAL GEOLOGY OF THE BALCONES IGNEOUS PROVINCE

The BIP extends across the Maverick Basin and the San Marcos Arch in South and Central Texas, covering an area of approximately 200 to 250 mi (320 to 400 km) in length and 10 to 40 mi (15 to 65 km) in width (Simmons, 1967) (Fig. 1). Ewing (1986) and Barker et al. (1987) documented more than 200 volcanic features in the area. Volcanic rocks in the BIP are silica-undersaturated and predominantly mafic tuffs in composition (e.g., Barker et al., 1987). Spencer (1969), Ewing and Caran (1982), Wittke and Lawrence (1993), Ewing (2004), Griffin et al. (2010), and Reed and Loucks (2022) presented more detailed information on the composition of these igneous rocks.

During Late Cretaceous Austin Chalk time the area of investigation was a drowned deep water platform, where marly chalks to chalky marls were deposited under environmental conditions ranging between oxic and anoxic (e.g., Loucks et al., 2020, 2022). The Maverick Basin had deeper water conditions than the San Marcos Arch, but both areas were below storm-wave base out on the platform (e.g., Loucks et al., 2020; Loucks and Reed, 2022).

In the Maverick Basin area, Ewing (2013) divided the Austin Chalk section into several stratigraphic units based on nomenclature used in the Pearsall field area (units AC–A through AC–E; Fig. 2). The AC–B1 unit contains numerous volcanic features, including pyroclastic talus mounds, dikes, and sills. The AC–A unit also appears to contain some volcanic sediments similar to the AC–B1 unit on and east of the San Marcos Arch. These volcanic features are localized, but associated volcanic ash-fall material is spread throughout the BIP area (Loucks and Reed, 2022). On the basis of Ar^{40}/Ar^{39} isotope ages, Griffin et al. (2010) proposed the timing of emplacement of the Austin-age intrusions in the AC–B1 unit as 84.1–81.5 Ma (during AC–B1 time; late Santonian to early Campanian).

UPPER AUSTIN CHALK—B1 LITHOFACIES

Figure 2 is the wireline log of the type Austin Chalk section proposed by Loucks et al. (2020) for the Maverick Basin area. The wireline log identifies the stratigraphic units within the Austin Chalk. These units can be correlated throughout the Maverick Basin, but they thin or pinch out east onto the San Marcos Arch and southeast against the raised relict topography of the Lower Cretaceous paleo–Stuart City Reef margin (Ewing, 2013; Loucks et al., 2020).

The AC–A and –B1 sections contain several rock types, including both sedimentary and volcanic lithofacies (Loucks et al., 2020, 2022; Loucks and Reed, 2022, 2023). The dominate lithofacies in the upper Austin Chalk units are lithofacies 1, 2, and 5 of Loucks et al. (2020), and are described later in this section. These lithofacies contain common to abundant sand-size glauconite grains (Figs. 3E and 3F).

No volcanic mound bodies were encountered in the investigated Austin Chalk cores; however, some of the cores are proximal to volcanic mounds, as indicated by wireline-log analysis and correlations and core samples containing abundant pyroclastic ash (Figs. 3E, 3F, and 4). The volcanic-rich lithofacies described in core are altered ash beds and ash-rich lime packstones and grainstones. On wireline logs, the altered volcanic material (transformed to clay minerals) is characterized by positive gam-

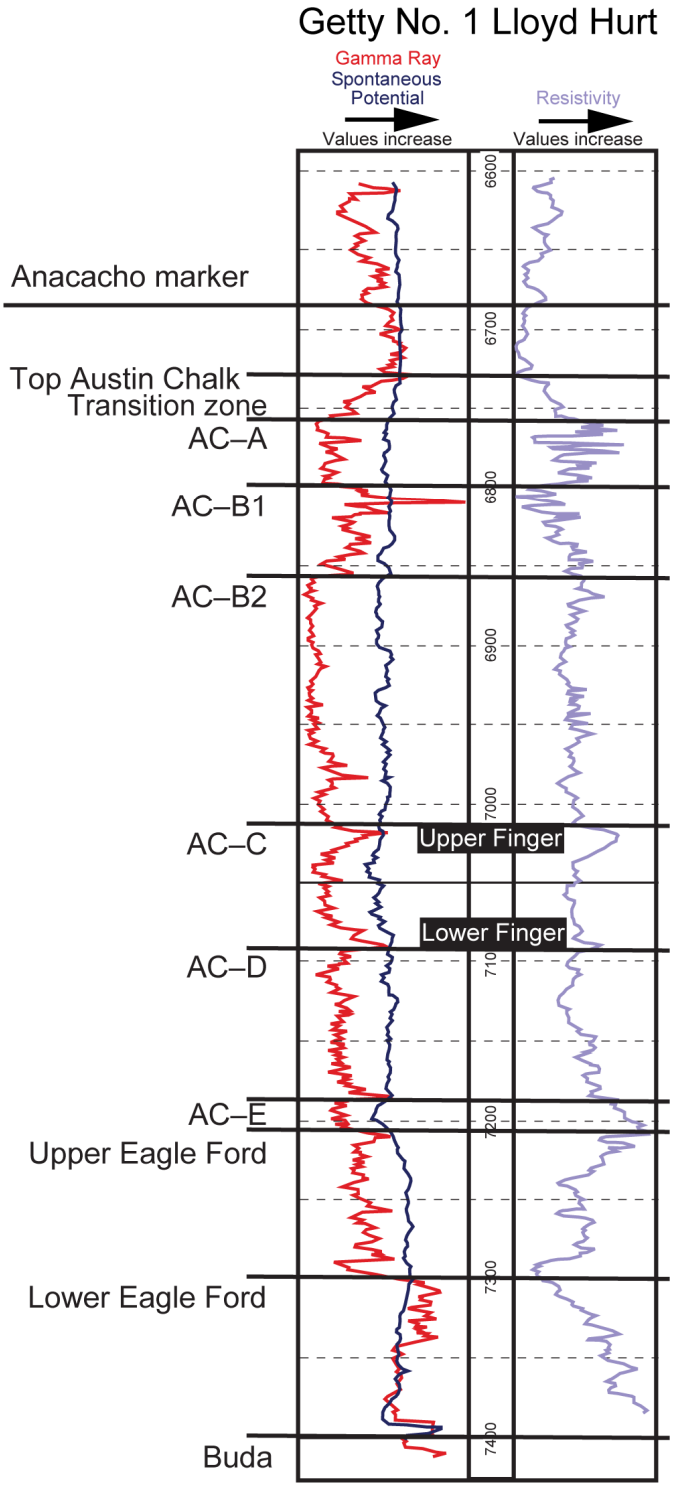

Figure 2. Wireline log of the Getty No. 1 Lloyd Hurt well in Dimmit County, Texas, displaying the Buda to Anacacho section. The Austin Chalk section is divided into units according to Ewing (2013). Core in this well covers the complete Austin Chalk section and has been designated the type core for the Austin Chalk in the Maverick Basin (Loucks et al., 2020).

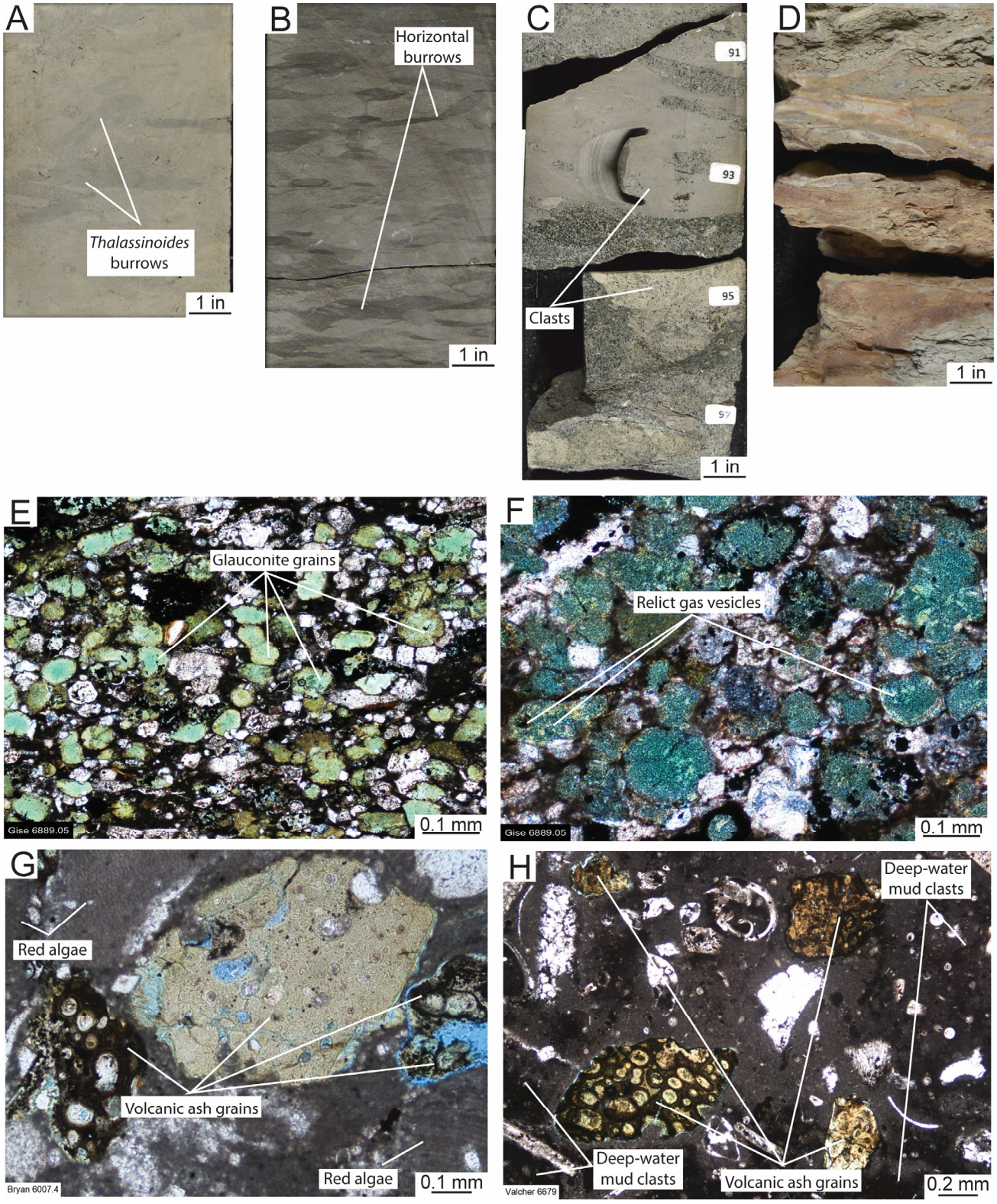

Figure 3. Examples of lithofacies in the AC–A and –B1 units. (A) Lithofacies 1: Burrowed argillaceous-poor marly chalk. Contains both oblique and horizontal burrows. Core. Tesoro No. 1 Clare, 1955 ft (595.9 m). (B) Lithofacies 2: Highly-burrowed, very-argillaceous chalky marl. All burrows are horizontal. Core. Evergreen Oil Corp. No. 1 Vicker Olyn, 5704 ft (1738.6 m). (C) Lithofacies 5: Debrite with large burrowed mud clast and several grain-rich clasts. Matrix is a glauconite-rich coccolith hash. Core. Tesoro No. 1 Valcher, 6621 ft (2018.0 m). (D) Highly-altered volcanic ash bed. Core. Tesoro No. 1 Valcher, 6892 ft (2100.7 m). (E) Sand-size rounded glauconite grains in a marly chalk that are interpreted to be volcanic ash in origin. This sample, from Dimmit County, is from a well not proximal to a known volcano. Thin section. Proco No. 1, Gise 6889 ft (1185.4 m). (F) Close up of same thin section shown in E with photomicrograph taken under cross-polarized light. Thin section. Proco No. 1 Gise, 6889 ft (1185.4 m). (G) Thin-section photomicrograph of a debrite with ash grains and red algae. Tesoro No. 1 Bryan, 6007 ft (1831.0 m). (H) Thin-section photomicrograph of a hyperconcentrated gravity flow with ash grains in a coccolith hash matrix. Tesoro No. 1 Valcher, 6679 ft (2035.8 m).

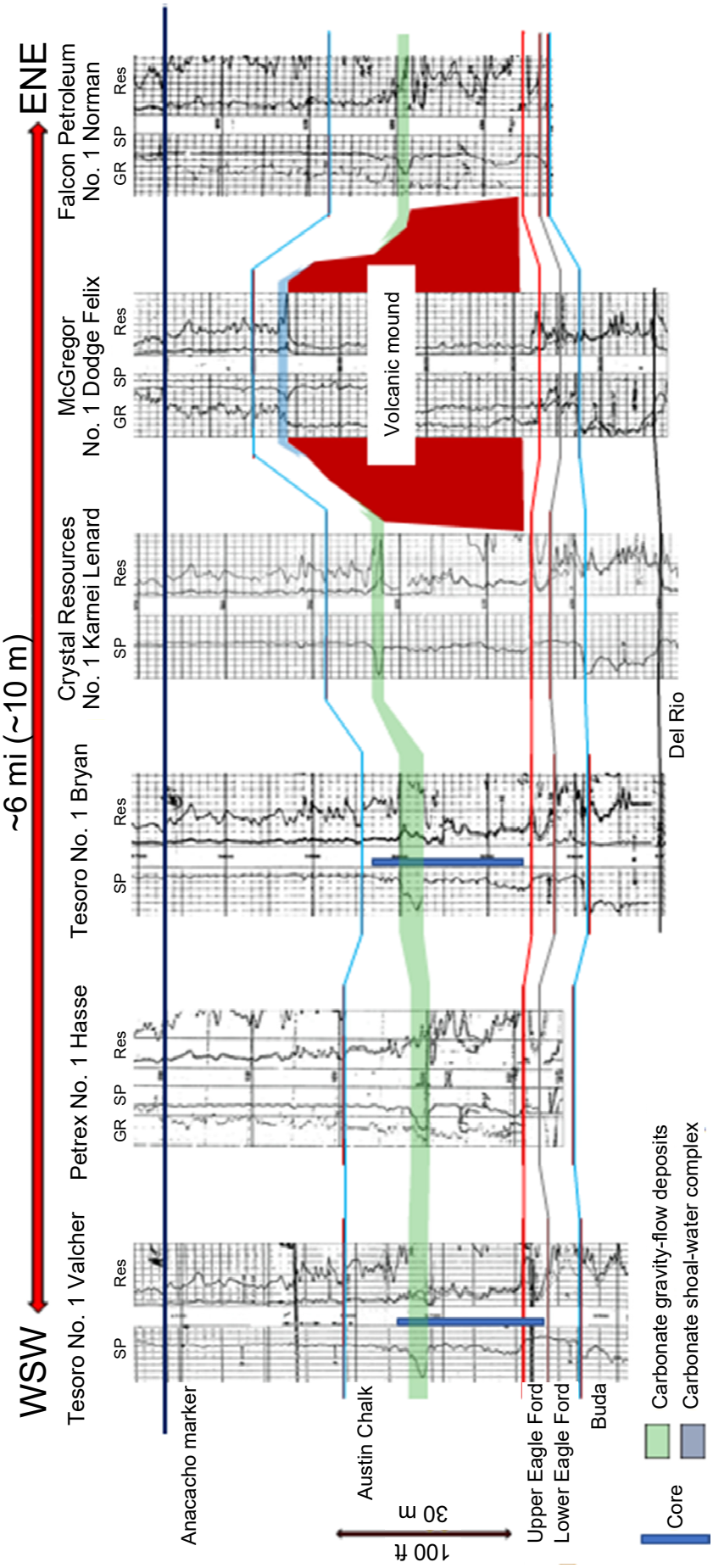

Figure 4. WSW–ENE cross-section displaying carbonate-grain-rich deposits associated with a volcanic mound. The blue lens is interpreted as a carbonate grainstone shoal complex on top of a volcanic mound, and the green lenses are gravity-flow deposits consisting of debrites and hyperconcentrated gravity flows with abundant shallow-water allochems and volcanic ash in which many of the ash grains are replaced by glauconite. Location of cross-section is shown in Figure 1.

ma-ray and spontaneous-potential curves and negative resistivity curves (Fig. 4) (see Thompson [2019, 2020, 2023] for other examples).

The volcanic-dominated lithofacies are abundant in two cores from Wilson County (Tesoro No. 1 Bryan and Tesoro No. 1 Valcher), where gravity-flow deposits proximal to a volcanic mound (North Pool area) were recovered (Fig. 4). They are ash-rich lime packstones and grainstones (i.e., debrites and hyperconcentrated-density-flow deposits) (Figs. 3E and 3F) and heavily altered ash beds (Fig. 3D). Volcanic-ash-rich debrites are composed of ash with a mixture of shallow-water biota and soft-lime-mud clasts (Fig. 3E).

Hyperconcentrated-density-flow deposits (i.e., deposited from a grain-rich gravity flow) having a packstone to grainstone texture occur in both wells noted above and are interpreted as having been deposited proximal to the base of a volcanic mound (Fig. 4). These deeper-water flow deposits contain a mixture of shallow- and deep-water biota with the addition of volcanic ash (Fig. 3F). The shallow-water formed biota consist of red and green algae, benthic foraminifers, echinoid fragments, oysters, ostracods, and rare corals, whereas the deep-water deposited biota consist of planktic foraminifers, calcispheres, saccocomids, coccolith hash, and inoceramid fragments. The volcanic components are ash (<2 mm) and rare lapilli (≥2 mm). The volcanic material was rapidly altered after ejection and contact with seawater (e.g., Spencer, 1969; Ewing, 1986; Mitchell-Tapping, 1988). Some ash-fall layers (up to 4 ft [1.2 m] thick) (Fig. 3D) are present in the investigated cores and contain altered to well-preserved former volcanic glass shards.

Lithofacies 1 is a highly burrowed marly chalk (Fig. 3A) with low total organic carbon (TOC) (mean = ~0.30 wt%) (Loucks et al., 2020). Burrows are horizontal to vertical. Predominant biota include planktic foraminifers, inoceramid fragments, calcispheres, and saccocomids in a coccolith-hash matrix. Rarer biota include echinoderm fragments, ostracod valves, oyster fragments, and benthic foraminifers. Lithofacies 2 is a very argillaceous, highly burrowed, marly chalk to chalky marl (Fig. 3B) with moderate TOC (mean = ~1.0 wt%) (Loucks et al., 2020). Biota are similar to those in lithofacies 1. Nearly all burrows are horizontal. Lithofacies 1 and 2 were deposited in place with minor resedimentation. Lithofacies 1 reflects a quiet-water, oxic bottom environment, whereas lithofacies 2 reflects a quiet-water, oxic to dysoxic bottom environment.

Lithofacies 5 was deposited by gravity-flow processes that produced debrites and hyperconcentrated-density-flow deposits. These deposits contains abundant glauconite (e.g., Fig. 3C). Two major types of debrites are present (Loucks and Reed, 2022). The first type is composed of soft-lime-mud intraclasts (i.e., mud not lithified at time of deposition), and the second type is composed of skeletal fragments of oysters or inoceramid fragments. The soft-mud clasts were mobilized from updip and carried downdip by debris-flow processes that can transport unlithified mud clasts with only minor distortion. The mud clasts were firm enough to preserve relict burrows but soft enough to be distorted. Some debrites, where the outlines of the mud clasts are not well defined, can be misinterpreted as burrowed firmgrounds or hardgrounds as noted by Loucks and Reed (2022).

Lithofacies 1, 2, and 5 are common in all 12 cores investigated (Loucks and Reed, 2022). Lithofacies 5 becomes much rarer in the AC–A and –B1 units in cores investigated outside the limits of the BIP (Loucks and Reed, 2022). Loucks and Reed (2022) postulated that gravity-flow deposits are related to resedimentation produced by earthquakes associated with volcanic eruptions or by large storms. Also, steeper mound slopes (up to 9 degrees) associated with volcanic mounds would promote soft-bottom sediment instability and favor resedimentation by gravity flow processes.

ALTERATION OF VOLCANIC ASH TO GLAUCONITE

Many of the samples in the AC–A and –B1 units show abundant glauconite grains that vary in shape and size (Figs. 5–11). A spectrum of glauconite grains are seen in two cores (No. 1 Valcher and No. 1 Bryan) proximal to a volcanic mound in the WSW–ENE cross-section (Fig. 4) and can be readily identified as replaced ash. However, in other areas distal to volcanic mounds, the altered ash is not as easily identified as volcanic in origin (e.g., Figs. 3E and 3F); evidence must be documented and integrated to establish and document their volcanic origin. To build evidence for the replacement of volcanic ash by glauconite, we first describe the macro-characteristics of the ash not altered to glauconite and then describe the ash that has been altered to glauconite as seen in the No. 1 Valcher and No. 1 Bryan cores. We then show the step-by-step transition of recognizable ash to glauconite-replaced ash that reveals no volcanic-origin evidence except that they are intimately associated with volcanic sediments and some have rare relict gas-vesicle structure. This procedure substantiates the transformation of volcanic ash to glauconite. We then compared the known glauconite-replaced ash to sediment that was deposited distal to a volcanic mound. Following the macro-characteristic description of the volcanic grains, a description of the microscale characteristics of the alteration processes and products were defined using SEM analysis.

As mentioned above, the No. 1 Valcher and No. 1 Bryan cores (Fig. 4) in Wilson County contain volcanic-rich lithofacies where ash is replaced by vermiculite and glauconite and, in some examples, phosphate and calcite. These two cores are located in an excellent area for investigating the transition from volcanic ash to vermiculite and glauconite as these cores contain volcanic ash at different stages of diagenesis. Figures 5–11 display examples of the spectrum of these ash grains.

Glauconite-Replaced Ash in the Proximal Area of a Volcanic Mound

The cross-section presented in Figure 4 shows a volcanic mound and interpreted associated carbonate deposits. A shallow-water carbonate shoal system is present at the top of the mound, and gravity-flow deposits occur at the base of and peripheral to the mound. The carbonate gravity-flow deposits in the No. 1 Valcher and No. 1 Bryan wells are displayed by low spontaneous potential (i.e., reflection to the left) curves, indicating less argillaceous carbonates. These gravity-flow units were cored in both

(FACING PAGE) Figure 5. Thin-section photomicrographs of well-preserved volcanic ash. All the ash grains appear to be abraded. (A) Complex ash grain with gas vesicles and cement. Tesoro No. 1 Valcher, 6679 ft (2035.8 m). (B) Ash with fibrous cement-filled gas vesicles. Tesoro No. 1 Bryan, 6007 ft (1831 m). (C) Ash with contorted fabric. Tesoro No. 1 Bryan, 6007 ft (1831 m). (D) Compacted dark ash grain showing flattened gas vesicles. Tesoro No. 1 Bryan, 6007 ft (1831 m). (E) Several ash grains. Ash grain on left shows gas vesicles, some being compacted. Grain is replaced by glauconite. Ash grain on right is very dark but shows outlines of gas vesicles. Tesoro No. 1 Bryan, 6007 ft (1831 m). (F) Ash grain with irregular outline. Fabric may be cemented fine-grained ash particles. Tesoro No. 1 Valcher, 6679 ft (2035.8 m). (G) Ash with well-rounded gas vesicles filled with fibrous cement. Tesoro No. 1 Valcher, 6679 (2035.8 m). (H) Gas vesicles filled with several stages of fibrous cement. Tesoro No. 1 Valcher, 6679 ft (2035.8 m).

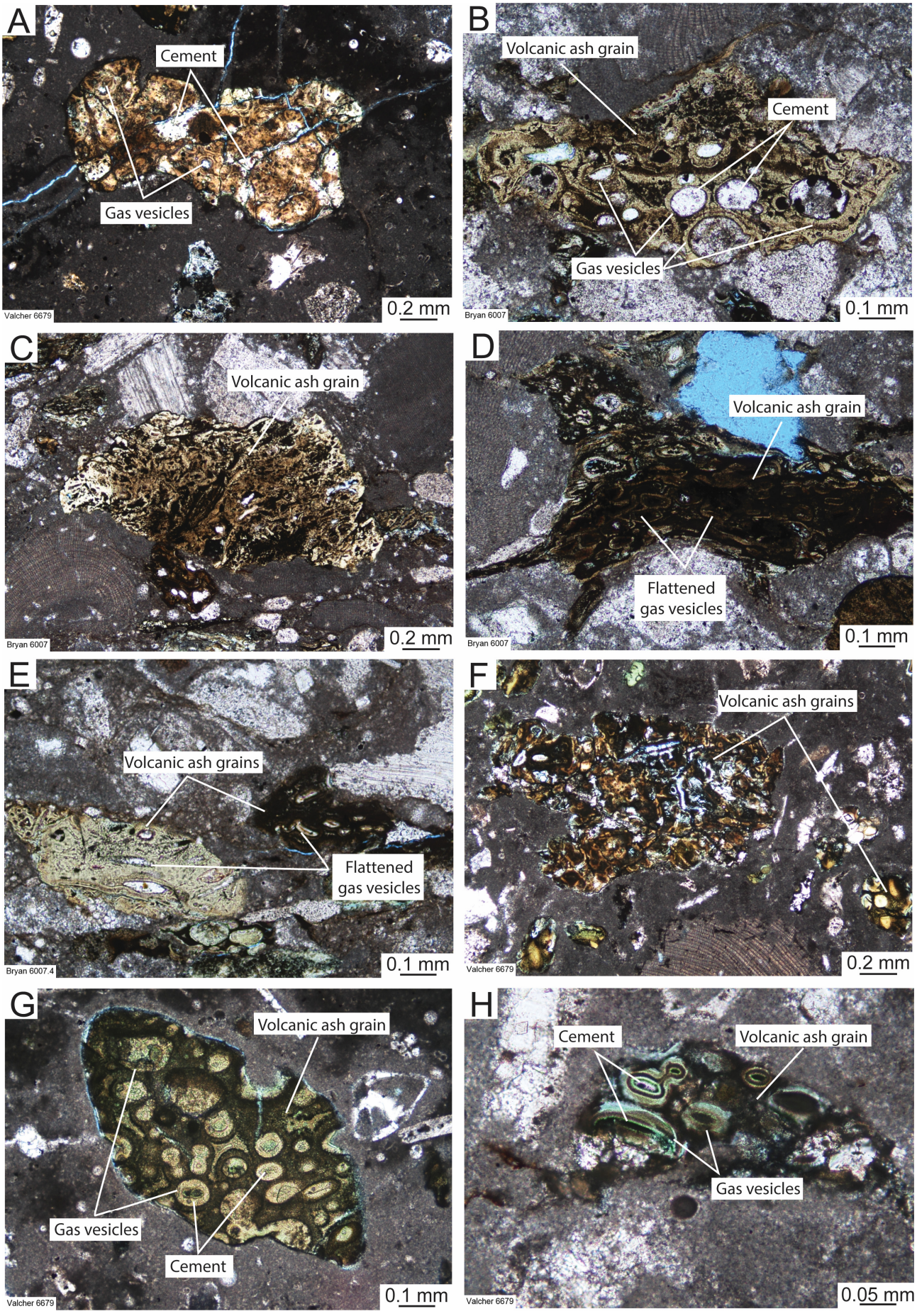
A
Cement
Gas vesicles
Valcher 6679
0.2 mm
B
Volcanic ash grain
Cement
Gas vesicles
Bryan 6007
0.1 mm
C
Volcanic ash grain
Bryan 6007
0.2 mm
D
Volcanic ash grain
Flattened gas vesicles
Bryan 6007
0.1 mm
E
Volcanic ash grains
Flattened gas vesicles
Bryan 6007.4
0.1 mm
F
Volcanic ash grains
Valcher 6679
0.2 mm
G
Volcanic ash grain
Gas vesicles
Cement
Valcher 6679
0.1 mm
H
Cement
Volcanic ash grain
Gas vesicles
Valcher 6679
0.05 mm

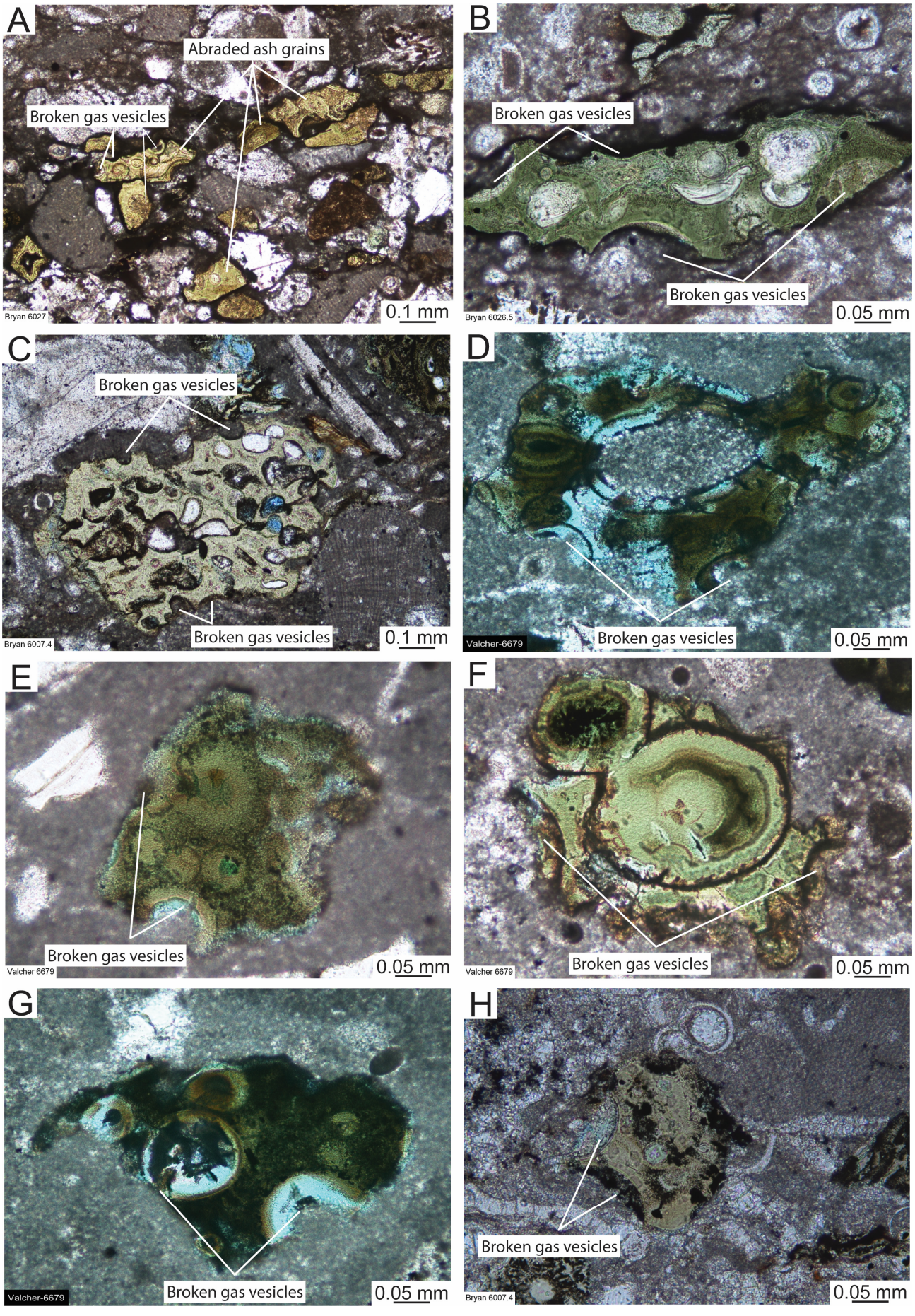
A
Abraded ash grains
Broken gas vesicles
Bryan 6027
0.1 mm
B
Broken gas vesicles
Broken gas vesicles
Bryan 6026.5
0.05 mm
C
Broken gas vesicles
Broken gas vesicles
Bryan 6007.4
0.1 mm
D
Broken gas vesicles
Valcher-6679
0.05 mm
E
Broken gas vesicles
Valcher 6679
0.05 mm
F
Broken gas vesicles
Valcher 6679
0.05 mm
G
Broken gas vesicles
Valcher-6679
0.05 mm
H
Broken gas vesicles
Bryan 6007.4
0.05 mm

(FACING PAGE) Figure 6. Thin-section photomicrographs of volcanic ash showing evidence of abrasion without much rounding. (A) Several ash grains showing broken gas vesicles. Tesoro No. 1 Valcher, 6679 ft (2035.8 m). (B) Angular glauconitic ash grain where broken gas vesicles outline the particle. Tesoro No. 1 Valcher, 6679 ft (2035.8 m). (C) Glauconitic ash with numerous broken gas vesicles at edge of particle. Tesoro No. 1 Valcher, 6679 ft (2035.8 m). (D) Well-abraded altered ash with preserved relict fibrous-cement-filled gas vesicles and several broken gas vesicles at edge of particle. Tesoro No. 1 Valcher, 6679 ft (2035.8 m). (E) Fine-grained glauconitic ash grain with cement-filled gas vesicles and broken gas vesicles at edge of particle. Tesoro No. 1 Valcher, 6679 ft (2035.8 m). (F) Well-abraded glauconitic ash grain composed of a few cement-filled gas vesicles. Outline of particle consists of broken gas vesicles. Tesoro No. 1 Valcher, 6679 ft (2035.8 m). (G) Well-abraded, dark-ash grain composed of whole and broken gas vesicles. Tesoro No. 1 Valcher, 6679 ft (2035.8 m). (H) Very small abraded glauconitic ash grain with various sized gas vesicles. Outline of particle consists of walls of broken gas vesicles. Tesoro No. 1 Bryan, 6007 ft (1831 m).

wells. The abundant volcanic ash in these deposits allows for the documentation of the transformation of the ash to pure glauconite silt and sand-size grains.

Volcanic Ash Grains

Figure 5 shows several examples of volcanic ash. As mentioned earlier, the initial volcanic lapilli and ash are altered early in seawater to various clay types (e.g., Spencer, 1969; Ewing, 1986; Mitchell-Tapping, 1988; Reed and Loucks, 2022). In the ash examples shown in Figure 5, all the ash grains show clear volcanic textures, and only one grain in Figure 5E is altered to glauconite based on color of grain. The major volcanic feature in the ash is gas vesicles that are generally filled with various cements. Some of the ash shows flattened gas vesicles (Figs. 5D and 5E). The ash grains also appear to be abraded, as indicated by broken gas vesicles at grain boundaries (e.g., Figs. 5B and 5G).

Highly Abraded Ash Grains

No lapilli were noted in the No. 1 Valcher and No. 1 Bryan cores, only ash. The cores are proximal to the base of the volcanic mound (Fig. 4) and we interpret that abrasion in shallow-water, higher energy environments and subsequent transport reduced the lapilli to ash-size grains. Also, some grain-size segregation likely occurred during transport. Figure 6 shows examples of well-abraded volcanic ash. The dominant evidence of abrasion is broken gas vesicles at the edges of the grain.

Relict Volcanic Textures

Figure 7 shows examples of volcanic ash that have transformed to glauconite grains. The glauconite is identifiable in thin section by its bright green color. The glauconite-replacement process may preserve relict features of the original volcanic texture or totally obscure the original volcanic texture. Figure 7A–7F shows grains with relict gas vesicles preserved to various degrees. In some samples the volcanic features have nearly vanished (e.g., Figs. 7C and 7D). Figure 7E is interesting in that a fine-sand-size grain of glauconite shows relict outlines of gas vesicles that are truncated at the grain boundary. Continued transformation to glauconite results in glauconite grains without any relict textures (Fig. 8).

Sand-Size Glauconite Grains

The most common glauconite grains in the AC–A and –B1 units are sand-size and reveal no or very rare and faint relict volcanic textures (Figs. 3F and 8A–8E). The grains are generally rounded (e.g., Figs. 8A–8D). These sand-size glauconite grains are common in the No. 1 Valcher and No. 1 Bryan cores, where they are associated with well-preserved volcanic grains that are in different stages of transformation to glauconite. The glauconite grains are present in all 12 cores investigated within the BIP (Loucks and Reed, 2022), but they are uncommon in the Austin Chalk outside the BIP (Fig. 1) or in other units in the Austin Chalk within the BIP. Rounded glauconite grains in Figure 3E and 3F are from the No. 1 Gise well in Dimmit County in the Maverick Basin, where the depositional site was not adjacent to a volcanic mound. The samples show abundant rounded sand-size glauconite grains with only rare and very faint gas-vesicle relict textures (Fig. 3F).

Figure 8E and 8F show complex replaced ash grains that may present some evidence of how the ash transformed to fine-grained, rounded glauconite. Grains in Figure 8E are composite glauconite grains in which further abrasion might fragment these grains into smaller rounded glauconite grains. Similarly, the ash grain in Figure 8F is a compound glauconite grain in which the gas vesicles are filled with glauconite. Fragmentation of this ash grain by abrasion could produce fine, rounded glauconite grains with no relict ash textures.

Scanning Electron Microscopy Analysis of Glauconite Replacement

SEM and EDS element mapping shows that the transformation from volcanic ash is not a single process, but it occurred in stages going from tuffs, to Na–rich, slightly devitrified basaltic glass (i.e., palagonite of Ewing [2004]), to vermiculite (probably mixed with smectite), and finally to glauconite and some phosphate. In this section the diagenetic transformation of ash to glauconite is documented at the microscale by analyzing SEM–EDS images of the transformation. A discussion of the chemistry of the diagenesis of the transformation process is beyond the scope, goals, and resources of this investigation.

Figure 9 shows several examples of the microscale transformation of volcanic ash to vermiculite and then to glauconite. The vermiculite-rich grains (greenish grains in Figures 9B–9D) show that parts of the gains have altered to glauconite (yellowish). This can be seen by the greenish color in the images mixed with the more yellowish color. The yellow signifies potassium in the glauconite. Ash that is totally converted to glauconite is bright yellow in the images (Fig. 9). All the partially replaced ash grains contain relict gas vesicles. The completely replaced glauconite grains appear homogenous and show no relict volcanic texture.

Figure 10 displays several SEM images of a volcanic ash fragment where glauconite and phosphate precipitation in pore spaces and has replaced the ash framework. The fragments show an irregular abraded outline and well-preserved gas vesicles (Fig. 10A). The pore spaces in the ash fragment is filled mainly by glauconite along with some calcite and phosphate (Figs. 10A and 10C). The glauconite in the gas vesicles has a branching fibrous fabric (similar to frost crystals or feathers) with micropores between the crystals (Figs. 10A and 10B). The phosphate in the grain is microgranular. Fine-crystalline calcite replaces the lower edge of the grain. Microcrystalline calcite in the lower left of the image is coccolith hash in the matrix.

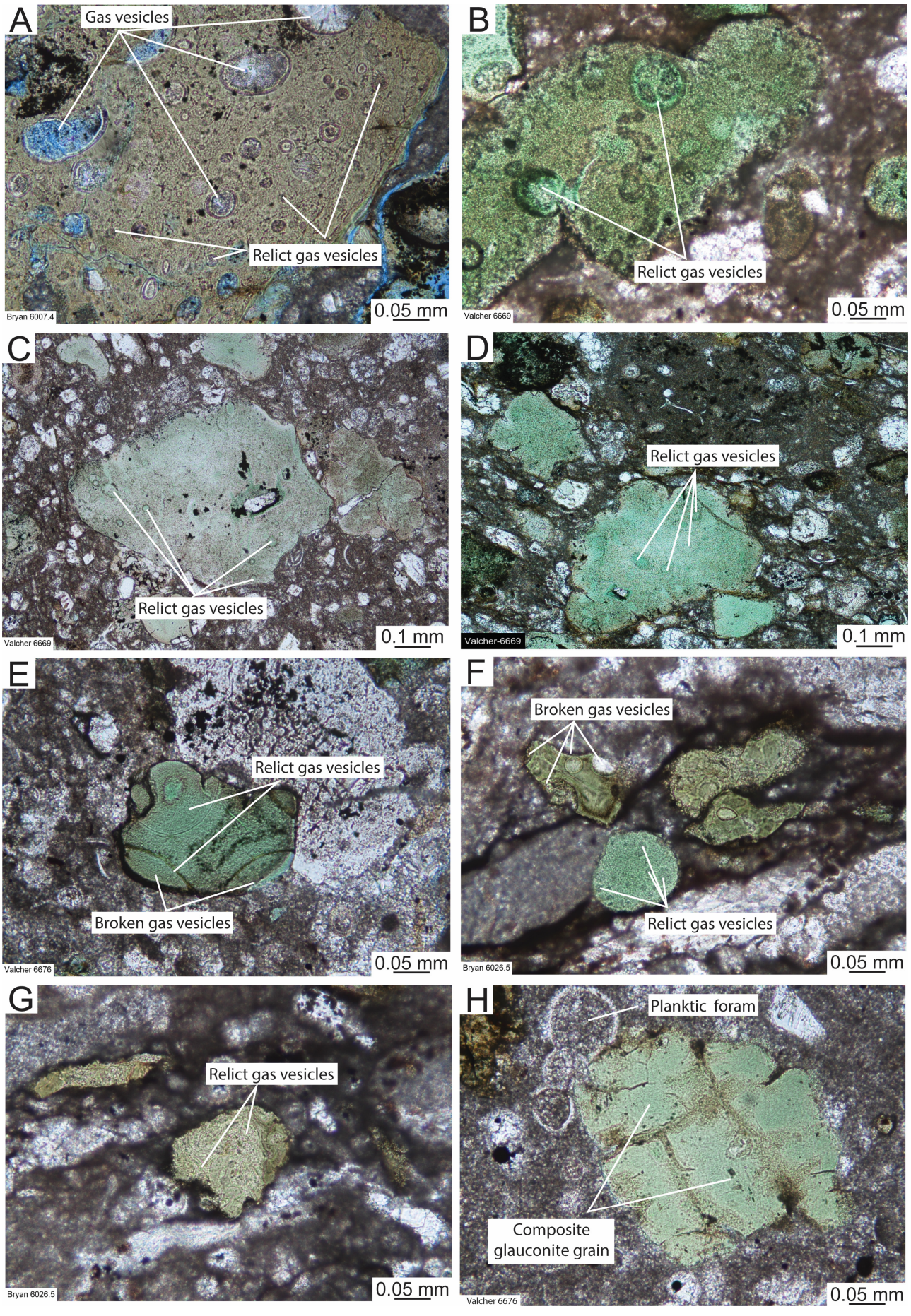
A
Gas vesicles
Relict gas vesicles
Bryan 6007.4
0.05 mm
B
Relict gas vesicles
Valcher 6669
0.05 mm
C
Relict gas vesicles
Valcher 6669
0.1 mm
D
Relict gas vesicles
Valcher-6669
0.1 mm
E
Relict gas vesicles
Broken gas vesicles
Valcher 6676
0.05 mm
F
Broken gas vesicles
Relict gas vesicles
Bryan 6026.5
0.05 mm
G
Relict gas vesicles
Bryan 6026.5
0.05 mm
H
Planktic foram
Composite glauconite grain
Valcher 6676
0.05 mm

(FACING PAGE) Figure 7. Thin-section photomicrographs of altered ash with relict volcanic texture. (A) Glauconitic ash showing some well-preserved gas vesicles along with many faint gas vesicles that were obscured by glauconite diagenesis. Tesoro No. 1 Valcher, 6669 ft (2032.7 m). (B) Glauconitic ash with relict gas vesicles. Tesoro No. 1 Valcher, 6669 (2032.7 m). (C) Glauconite-replaced ash grain with very faint gas vesicles. Tesoro No. 1 Valcher, 6676 ft (2035.8 m). (D) Several glauconite-replaced ash grains showing a few relict gas vesicles. Tesoro No. 1 Valcher, 6669 ft (2032.7 m). (E) Fine ash replaced by glauconite showing relict gas vesicles. Tesoro No. 1 Valcher, 6676 ft (2035.8 m). (F) Several glauconite ash grains showing well-preserved gas vesicles and a well-rounded glauconite-replaced ash grain with relict gas vesicles. Tesoro No. 1 Bryan, 6028 ft (1837.3 m). (G) Glauconite-replaced ash showing faint numerous outlines of relict gas vesicles. Tesoro No. 1 Bryan, 6028 ft (1837.3 m). (H) Glauconite-replaced ash grain with crude rectangular pattern that may reflect original lapilli structure. Tesoro No. 1 Valcher, 6676 ft (2035.8 m).

DISCUSSION AND CONCLUSIONS

Evidence has been presented in this investigation that shows the step-by-step replacement of volcanic ash with glauconite. These steps are summarized in Figure 11, which shows the breakdown of ash grains by abrasion that produces silt- to sand-size grains. The volcanic grains are replaced by vermiculite and then glauconite with some relict volcanic texture preserved. Further abrasion and replacement by glauconite result in rounded silt-to-sand-size glauconite grains that are found throughout the BIP in the AC–A and –B1 units.

Understanding the origin of the glauconite grains is important in documenting the stratigraphy of the Austin Chalk section, especially during the time of the AC–A and –B1 unit deposition. As has been well documented by several studies (Griffin et al., 2010; Ewing, 2013; Loucks et al., 2020; Loucks and Reed, 2022), the AC–A and –B1 units were deposited at a time of active volcanism. During this time of volcanism, increased slope angles existed near the volcanic mounds, creating positive conditions for gravity-flow deposition triggered by earthquakes off the mounds (Loucks and Reed, 2022). Many of these gravity-flow deposits were composed of soft-mud clasts that were deformed during transport, but they were firm enough to retain their general shape and preserve relict burrows. In the cores investigated by Loucks and Reed (2022), there is a range of debrites: many clasts are clearly visible, whereas other clast outlines are indeterminate. Debrites with large mud clasts, relative to the core width, may be misinterpreted as hardgrounds, but close inspection would reveal that the mud clasts are distorted and that some of the relict burrows in the clasts are truncated and some are upside down.

Moreover, misinterpreting the volcanic glauconite as sedimentary in origin (i.e., associated with hardgrounds) further confuses upper Austin Chalk sedimentology. It is well documented in the literature that glauconite can be a replacement product of volcanic ash grains (e.g., Mishra and Sen, 2018). As an example of the misinterpretation of the AC–B1 debrites as hardgrounds and volcanic glauconite as sedimentary glauconite, Griffith et al. (2022, 2023) proposed the AC–B1 unit as a transgressive system, on the basis of their interpretation of hardgrounds and sedimentary glauconite. No mention of the abundant volcanism in the AC–B1 unit was made, even though they used the No. 1 Valcher core (same core used in this investigation) as a key core. If the volcanism had been addressed, a different interpretation might have been presented.

The upper Austin Chalk section has a complex history of deeper water chalk deposition with penecontemporaneous volcanism. This volcanism produced a sedimentary depositional style different from general deeper water chalk deposition. Specifically, increased slopes near the volcanos produced numerous and large gravity-flow deposits. Moreover, the volcanic ash transforming to glauconite produced a major grain type. Both of these factors must be taken into consideration when constructing the depositional history of the upper Austin Chalk section.

The literature contains a number of publications where glauconite grains (i.e., pellets) are associated with volcanic sediments (e.g., Bitschene et al., 1992; Geptner, et al., 2008; Abas, 2014). Our investigation suggests that in areas where volcanism and glauconite occur, a detailed investigation is necessary to document the origin of the glauconite and not assume it is sedimentary glauconite.

ACKNOWLEDGMENTS

We thank the State of Texas Advanced Resource Recovery (STARR) program and the Carbonate Reservoir Characterization Research Laboratory (RCRL) at the Bureau of Economic Geology, The University of Texas at Austin, for their support of this investigation. Amanda R. Masterson copyedited this manuscript. Priyanka Periwal helped with SEM sample preparation. Publication authorized by the Director, Bureau of Economic Geology, Jackson School of Geosciences, The University of Texas at Austin.

REFERENCES CITED

Abas, R. M., 2014, Glauconitic laminated crusts from hydrothermal alteration of Jurassic pillow-lavas (Betic Cordillera, S. Spain): A microbial influence case: Journal of Iberian Geology, v. 40, p. 389–408, <https://doi.org/10.5209/rev-_JIGE.2014.v40.n3.43080>.

Barker, D. S., R. H. Mitchell, and D. McKay, 1987, Late Cretaceous nephelinite to phonolite magmatism in the Balcones province, Texas, *in* E. M. Morris and J. D. Pasteris, eds., Mantle metasomatism and alkaline magmatism: Geological Society of America, v. 215, p. 371–374, <https://doi.org/10.1130/SPE215-p293>.

Bitschene, P. R., M. A. Holmes, and J. R. Breza, 1992, 9. Composition and origin of Cr–rich glauconitic sediments from the southern Kerguelen Plateau (site 748): Proceedings of the Ocean Drilling Program, Scientific Results, v. 120, p. 113–134.

Ewing, T. E., 1986, Balcones volcanoes in South Texas—Exploration methods and examples, *in* E. L. Stapp, ed., Contributions to the Geology of South Texas: South Texas Geological Society, p. 368–379.

Ewing, T. E., 2004, A nonspecialist's guide to the volcanology and petrology of the Balcones Igneous Province, *in* T. E. Ewing, ed., Volcanoes, asphalt, tectonics and groundwater in the Uvalde area, southwest Texas: South Texas Geological Society Guidebook 2004–1, p. 24–34.

Ewing, T. E., 2013, Stratigraphy of the Austin, Eagle Ford, and Anacacho formations and its influence on hydrocarbon resources, Pearsall Field area, South Texas: Gulf Coast Association of Geological Societies Transactions, v. 63, p. 213–225.

Ewing, T. E., and S. C. Caran, 1982, Late Cretaceous volcanism in South and Central Texas: Stratigraphic, structural, and seismic models: Gulf Coast Association of Geological Societies Transactions, v. 32, p. 137–145.

Geptner, A. R., T. A. Ivanovskaya, E. V. Pokrovskaya, and N. P. Kuralenko, 2008, Glauconite from Paleogene volcanoterrigenous rocks in western Kamchatka: Lithology and Mineral Resources, v, 43, p. 228–249, <https://doi.org/10.1134/S0024490208030036>.

Griffin, W. R., K. A. Foland, R. J. Stern, and M. I. Leybourne, 2010, Geochronology of bimodal alkaline volcanism in the Balcones

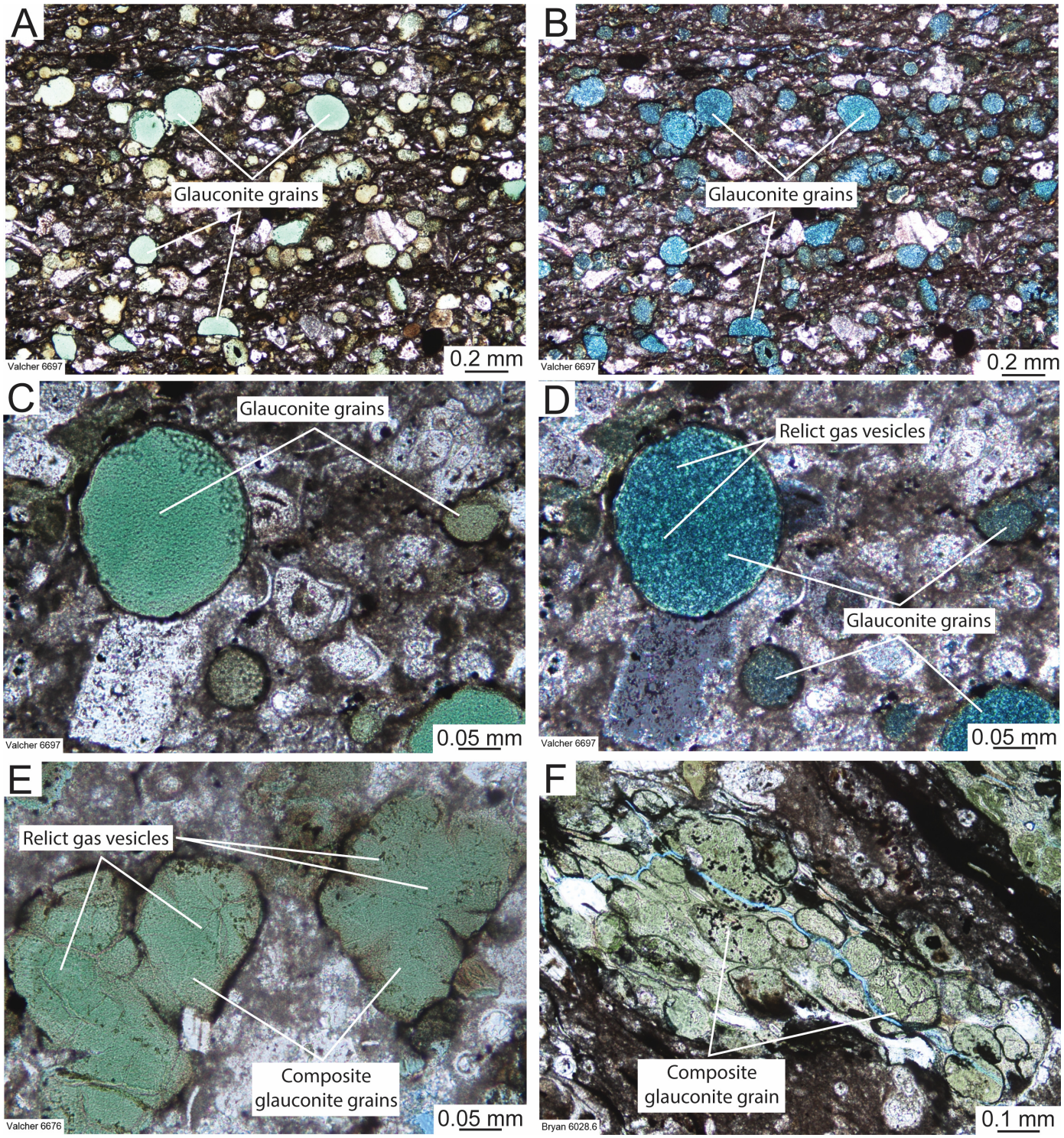

Figure 8. Thin-section photomicrographs of abraded and rounded glauconitic-ash grains that lack or have rare relict gas-vesicle structures. (A) Sand-size rounded glauconite grains in marly chalk that are interpreted to be volcanic ash in origin. This sample is near a volcanic mound in Wilson County (Fig. 4). Tesoro No. 1 Valcher, 6697 ft (2041.2 m). (B) Same as A but photomicrograph taken under cross-polarized light. Tesoro No. 1 Valcher, 6697 ft (2041.2 m). (C) Closeup of rounded glauconite-replaced ash with no relict ash structures in plane-polarized light. Tesoro No. 1 Valcher, 6697 ft (2041.2 m). (D) Same as C but photomicrograph taken under cross-polarized light. Some faint internal rounded features may be relict gas vesicles. Tesoro No. 1 Valcher, 6697 ft (2041.2 m). (E) Irregular volcanic grains replaced by glauconite showing very faint relict gas vesicle structures. If these grains were to have broken down into discrete particles and become more rounded, they would be similar to the glauconite grains shown in A and C. Tesoro No. 1 Valcher, 6676 ft (2035.0 m). (F) Ash grain with gas vesicles filled with glauconite. The fragmentation of this composite grain could produce rounded glauconite grains similar to those in A and C. Tesoro No. 1, Bryan 6028 ft (1837.3 m).

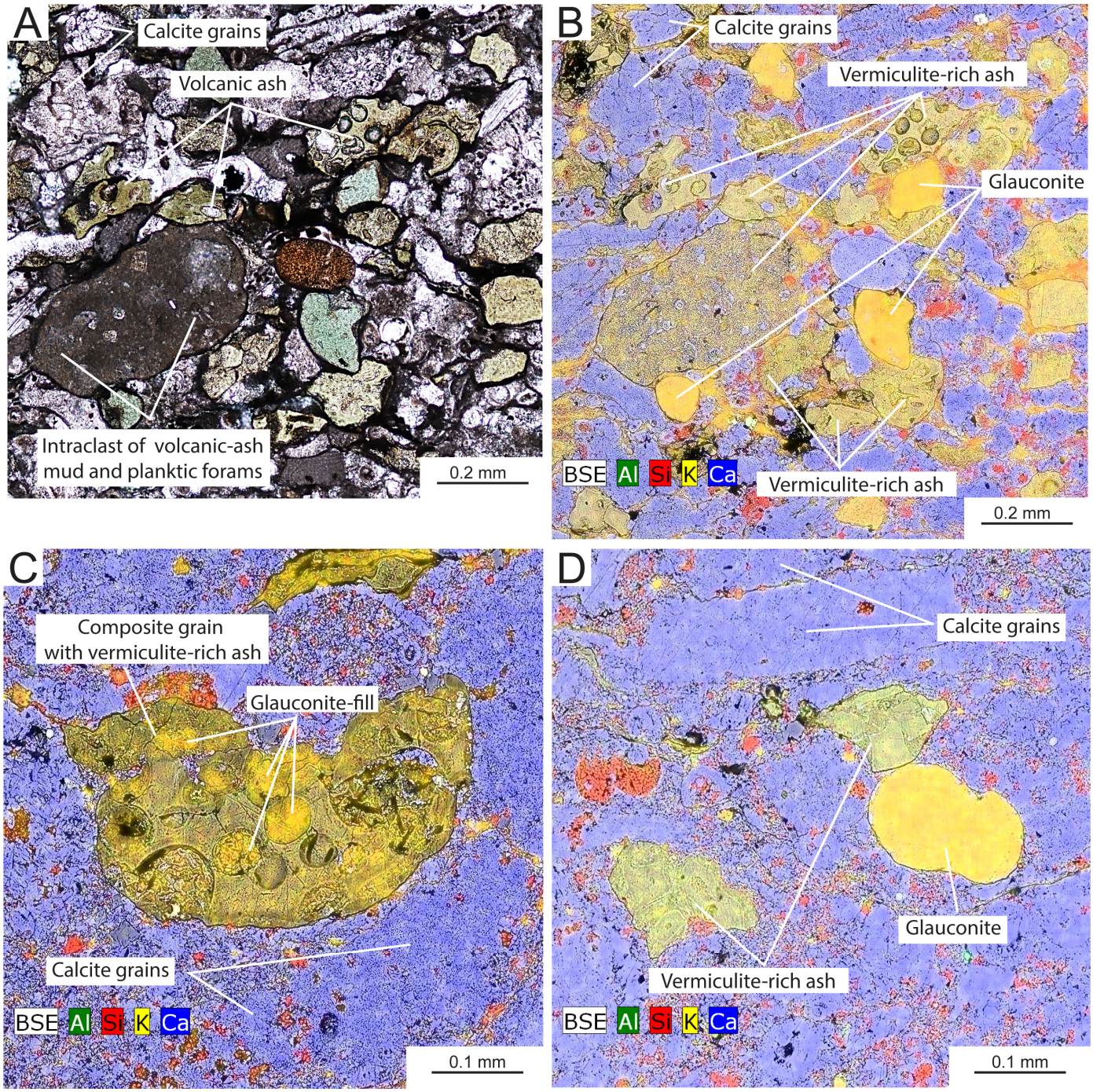

Figure 9. Scanning electron microscopy and energy dispersive spectroscopy element maps of volcanic ash transforming to vermiculite and glauconite. (A) Mixed carbonate and volcanic ash grains. Some of the ash contains gas vesicles. Varying shades of green in the ash indicate varying amounts of glauconite replacement. Dark grain in left central of the photomicrograph is an intraclast composed of altered volcanic-ash mud and some microfossils. Figure B is an EDS–SEM image of this thin-section area. Thin section. Tesoro No. 1 Bryan, 6028 ft (1837.3 m). (B) Same area as A. EDS elemental map showing mixture of carbonate and volcanic grains. The volcanic ash grains are in various stages of having transformed to vermiculite (greenish areas are vermiculite) and then to glauconite (yellowish areas are glauconite). The bright yellow grains are pure glauconite. EDS–SEM image. Tesoro No. 1 Bryan, 6028 ft (1837.3 m). (C) EDS element map of composite grain with volcanic ash grains showing differing degrees of alteration to glauconite. More greenish areas show replacement by vermiculite. More yellowish areas have more potassium, indicating that these areas have been converted to glauconite. Several vesicles are filled with glauconite (yellow) cement. EDS–SEM image. Tesoro No. 1 Bryan, 6007 ft (1830.9 m). (D) EDS element map of several volcanic ash grains with relict vesicles replaced by vermiculite (greenish) and glauconite (yellowish). The yellow glauconite grains shows no relict volcanic texture. EDS–SEM image. Tesoro No. 1 Bryan, 6026 ft (1836.7 m).

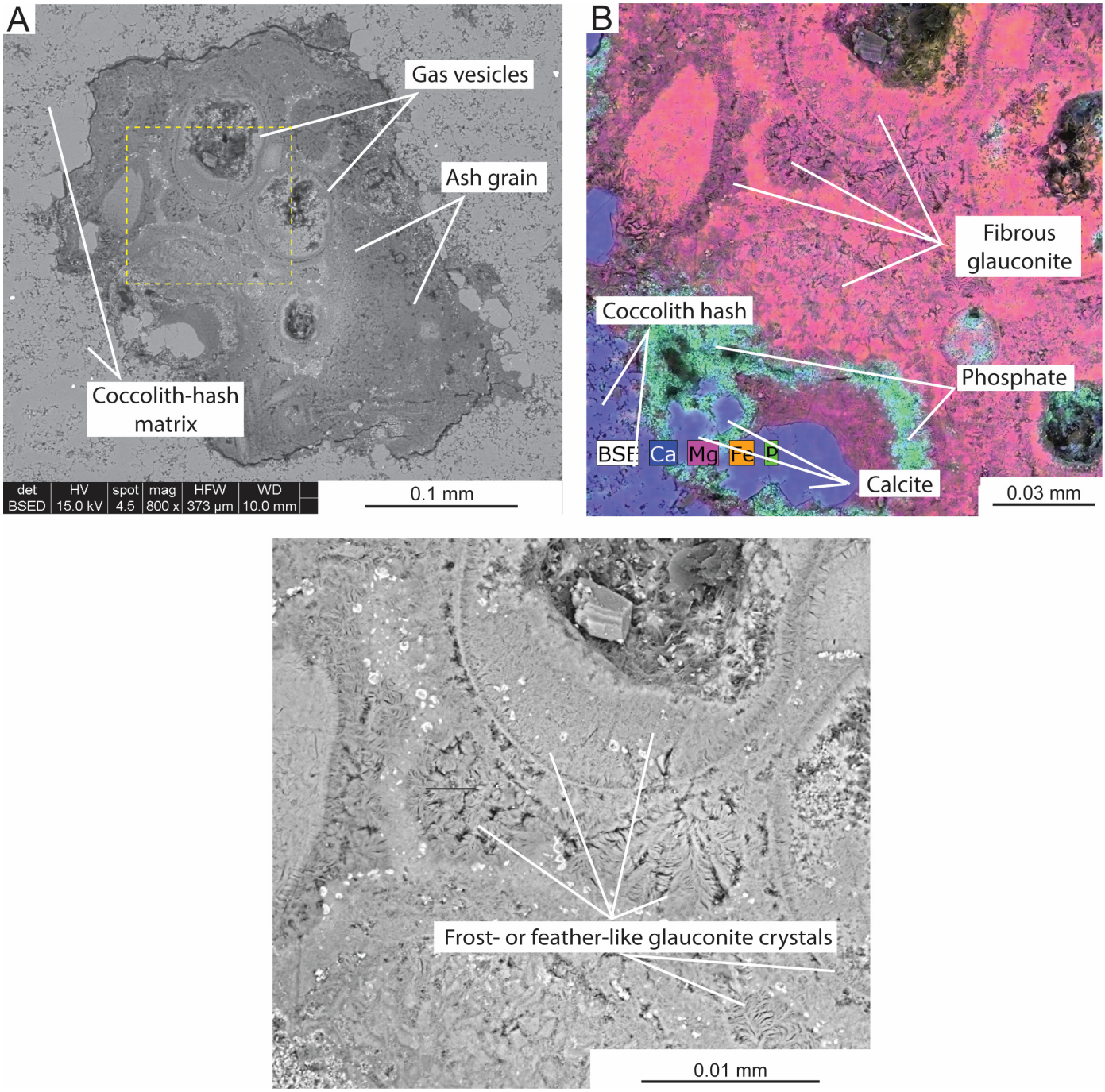

Figure 10. Backscattered electron images of Tesoro No. 1 Valcher, 6679 ft (2035.8 m). (A) Volcanic ash grain replaced mainly by glauconite, calcite, and phosphate and pores filled with glauconite. Well-developed gas vesicles in ash. (B) Energy dispersive spectrometry element map of part of A. (C) Closeup of yellow box in A showing frost- or feather-like glauconite crystals.

Igneous Province, Texas: Implications for Cretaceous intraplate magmatism in the Northern Gulf of Mexico magmatic zone: Journal of Geology, v. 118, p. 1–21, <https://doi.org/10.1086/648532>.

Griffith, C., J. Pospichal, E. de Kaenel, M. Pope, and A. Donovan, 2022, Regional sequence stratigraphy and biostratigraphic correlations of the Upper Cretaceous Austin Chalk in South and Central Texas: Insights into the evolution of the San Marcos Arch: Second International Meeting for Applied Geoscience and Energy, p. 3543–3545, <https://doi.org/10.1190/image2022-3749638.1>.

Griffith, C., J. Pospichal, E. de Kaenel, M. Pope, and A. Donovan, 2023, Regional sequence stratigraphy, biostratigraphy, facies, and depositional environments of the Upper Cretaceous Austin Chalk in South and Central Texas: GeoGulf Transactions, v. 72, p. 81–93.

Lonsdale, J. T., 1927, Igneous rocks of the Balcones Fault region of Texas: University of Texas Bulletin 2744, 178 p.

Loucks, R. G., S. Peng, K. E. Hattori, P. Periwal, J. R. Lambert, C. K. Zahm, and L. T. Ko, 2022, Depositional systems, lithofacies, and reservoir characterization of the Upper Cretaceous Austin Chalk, Brookeland and Burr Ferry fields, East Texas and

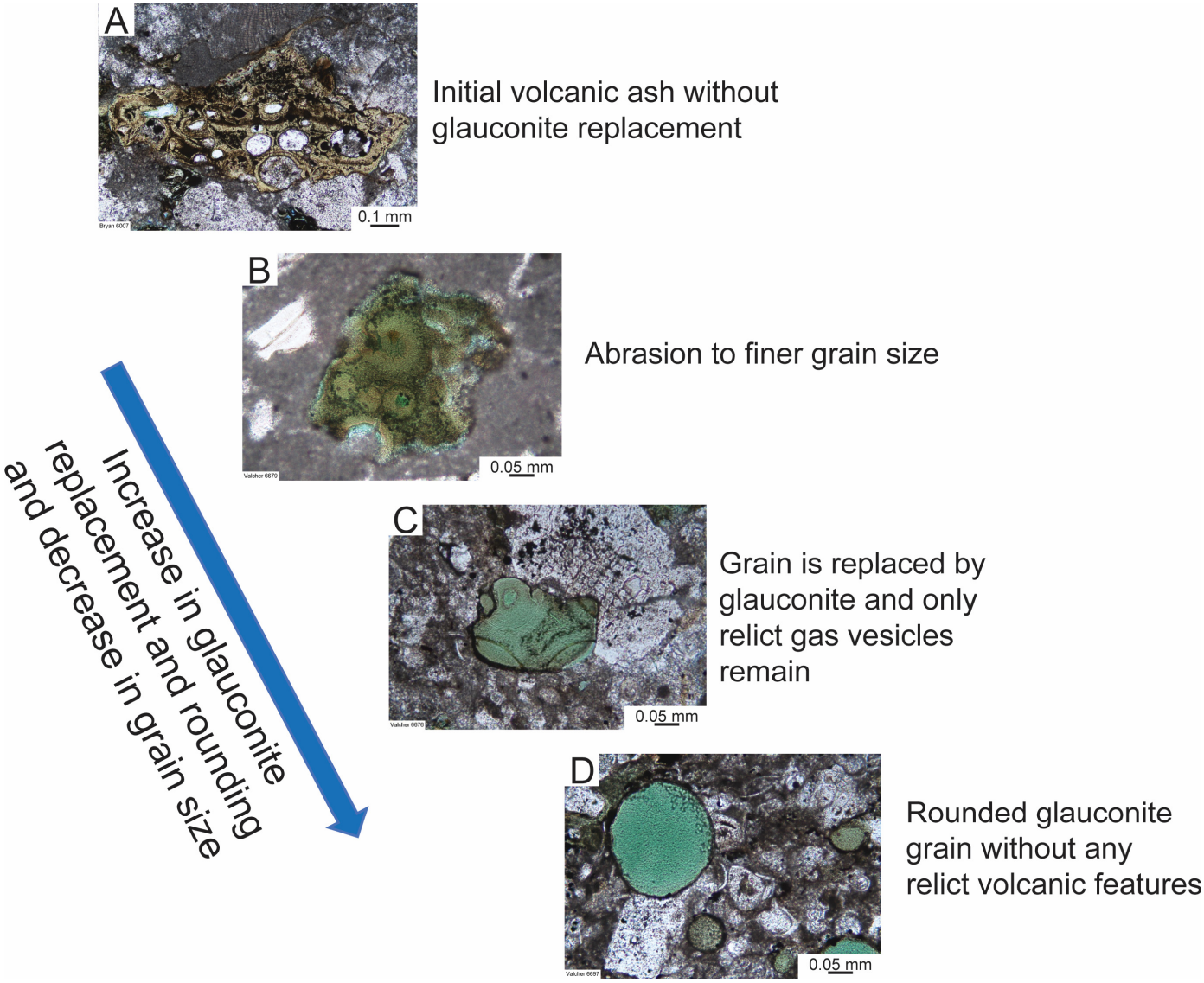

Figure 11. General stages of the transformation of volcanic ash to rounded glauconite grains (i.e., pellets). (A) Initial volcanic ash grain. (B) Abrasion of ash to a reduced size. Broken gas vesicles at grain boundaries are common. (C) Glauconite-replaced grain with some relict gas vesicles present. (D) Rounded and complete glauconite replacement of grain.

western Louisiana: Gulf Coast Association of Geological Societies Journal, v. 11, p. 37–57.

Loucks, R. G., and R. M. Reed, 2022, Implications for carbonate mass-wasting complexes induced by volcanism from Upper Cretaceous Austin Chalk strata in the Maverick Basin and San Marcos Arch areas of south-central Texas, USA: Sedimentary Geology, v. 432, 18 p., <https://doi.org/10.1016/j.sedgeo.2022.106120>.

Loucks, R. G., and R. M. Reed, 2023, Alteration of volcanic grains to glauconite in the Upper Cretaceous Austin Chalk Formation in the Balcones Igneous Province, South and Central Texas: GeoGulf Transactions, v. 72, p. 149–154.

Loucks, R. G., T. E. Larson, Y. Z, Zheng, C. K. Zahm, L. T. Ko, J. E. Sivil, S. Sheng, S. C. Ruppel, and W. A. Ambrose, 2020, Geologic characterization of the type cored section for the Upper Cretaceous Austin Chalk Group in South Texas: a combination fractured and unconventional reservoir: American Association of Petroleum Geologists Bulletin, v. 104, p. 2209–2245, <https://doi.org/10.1306/04222019197>.

Luttrell, P. E., 1977, Carbonate facies distribution and diagenesis associated with volcanic cones—Anacacho Limestone (Upper Cretaceous), Elaine Field, Dimmit County, Texas, *in* D. G. Bebout and R. G. Loucks, eds., Cretaceous carbonates of Texas and New Mexico—Applications to subsurface exploration: Bureau of Economic Geology Report of Investigations 89, p. 260–285, <https://doi.org/10.23867/RI0089D>.

Mishra, M., and S. Sen, 2018, Petrological study of the early Mesoproterozoic glauconitic sandstone and Olive Shale members from the Semri Group, Vindhyan Supergroup in central India: Implications to input from intrabasinal felsic volcanic source and glauconitization: Geological Journal, v. 158, p. 857–876, <https://doi.org/10.1002/gj.2931>.

Mitchell-Tapping, H. J., 1988, Exploration petrophysics of the "Serpentine" plugs of Texas: The Log Analyst, v. 29, no. 3, p. 186–203.

Reed, R. M., and R. G. Loucks, 2022, Textures, mineralogy, and reservoir properties of an altered mafic tuff core from the Upper Cretaceous (Lower Campanian) of Central Texas: Gulf Coast Association of Geological Societies Journal, v. 11, p. 1–15.

Saribudak, M., 2016, Near-surface geophysical mapping of an Upper Cretaceous submarine volcanic vent in Austin, Texas, USA: The Leading Edge, v. 35, p. 936–944, <https://doi.org/10.1190/tle35110986.1>.

Simmons, K. A., 1967, A primer on "serpentine plugs" in South Texas, *in* W. G. Ellis, ed., Contributions to the Geology of South Texas: South Texas Geological Society p. 125–132.

Spencer, A. B., 1969, Alkalic igneous rocks of the Balcones Province, Texas: Journal of Petrology, v. 10, p. 272–306, <https://doi.org/10.1093/petrology/10.2.272>.

Thompson, M. E., 1986, Stratigraphy of the Dale Lime and its relation to structure at Bateman Field, Bastrop County, Texas, *in* W. L. Stapp, ed., Contributions to the Geology of South Texas: South Texas Geological Society, p. 356–367.

Thompson, M. E., 2019, A revised age range for Texas Gulf Coast serpentine mounds: South Texas Geological Society Bulletin, v. 60, no. 5, p. 19–33.

Thompson, M. E., 2020, Alta Vista, Philtop, and Rinehart oil fields, Bexar County, Texas: South Texas Geological Society Bulletin, v. 61, no. 1, p. 15–32.

Thompson, M. E., 2023, Age of the Balcones Igneous Province, South-Central Texas: Additional revisions: GeoGulf Transactions, v. 72, p. 215–227.

White, R. H. Jr., 1960, Petrology and depositional pattern in the Upper Austin Group, Pilot Knob area, Travis County, Texas: Master's Thesis, University of Texas at Austin, 132 p.

Wittke, J. H., and L. E. Lawrence, 1993, OIB–like mantle source for continental alkaline rocks of the Balcones Province, Texas: Trace-element and isotopic evidence: Journal of Geology, v. 101, p. 333–344, <https://doi.org/10.1086/648227>.

Young, K. P., S. C. Caran, and T. E. Ewing, 1981, Cretaceous volcanism in the Austin area, Texas: Austin Geological Society Guidebook 4, 68 p.